# Thiadiazole containing N- and S-rich highly ordered periodic mesoporous organosilica for efficient removal of Hg(II) from polluted water

Surajit Das, Sauvik Chatterjee, Saptarsi Mondal, Arindam Modak, Bijan Krishna Chandra, Suparna Das, Gilbert Daniel Nessim, Adinath Majee and Asim Bhaumik*

## Electronic Supporting information

## Table of Contents



## Section S1

### Experimental Section

1,3,4-Thiadiazole-2,5-dithiol, (3-choloropropyl) triethoxy silane, tetraethyl orthosilicate, CTAB, tartaric acid and mercuric nitrate were purchased from Sigma Aldrich. Loba Chemie supplied the sodium methoxide. Dry methanol was received from Spectrochem, India. All other solvents and chemicals are bought from local commercial sources.

**Synthesis of bridging organosilane source (Z):**

All the reactions were carried out in oven dried glass apparatus under an inert atmosphere. Methanol was dried through the conventional procedure before using. To a mixture of 1,3,4-thiadiazole-2,5-dithiol (93 mg, 0.62 mmol) in 5 mL distilled methanol , 3.5 mL, 0.5M methanolic solution of MeONa was added and stirred at room temperature. After 10 min, a solution of (3-choloropropyl) triethoxy silane (313.04 mg, 1.3 mmol) in distilled MeOH (3ml) was added dropwise for half an hour to the thiadiazole mixture through a dropping funnel and stirring was continued at 60 $^0$C for 6 h. After complete addition the reaction mixture was slightly acidified, cooled down to room temperature and anhydrous $Na_2SO_4$ was added into it, shaken for 5 min and quickly filtered through a short column to produce a yellow colored solution. The reaction mixture was then concentrated by removing excess methanol to produce a highly viscous yellowish liquid. Yield: 68%. This as synthesized bridging organosilane precursor was designated as Z which is highly sensitive to air and moisture. This Z was characterized by $^1$H NMR (Figure S1). $^1$H NMR (400 MHz, DSMO-$d_6$) $\delta$ = 0.68 (t, J = 2.0 Hz, 2H), 1.15 (t, J = 2.0 Hz, 3H), 1.72-1.79 (m, 2H), 3.61 (t, J = 2.0 Hz, 2H), 3.75 (q, J = 2.0 Hz, 2H) ); FT-IR [$\tilde{\upsilon}$ (cm$^{-1}$)]: 3360 (s, br), 2974 (m), 2937 (m), 2837 (m) 2339 (w), 2099 (w), 1590 (s), 1448 (m),1416 (m), 1387 (m), 1352 (w), 1283 (m), 1166 (m), 1089 (vs), 1016 (vs), 956 (m), 863 (w), 786 (s), 706 (s).

**Synthesis of thiol rich DMTZ-PMO material:**

We have employed an optimum molar ratio of Z (organosilane precursor bearing two Si-units) to the pure silica cross-linker tetraethyl orthosilicate (TEOS) as 1:1 to obtain the hybrid material DMTZ-PMO. Initial pH of the reaction mixture was adjusted by using tartaric acid. Cetyltrimethylammoniumbromide (CTAB) was used as structure directing agent. In a typical synthesis, 1.02 g (2.8 mmol) of CTAB was dissolved in a previously prepared aqueous solution of tartaric acid (0.15 g TA in 6.5 g of H2O) and the whole solution was under continuous stirring at

room temperature for half an hour. A freshly prepared organosilane precursor Z (1.17 g, 2 mmol) and TEOS (0.41 g, 2 mmol) is mixed together in 5 ml of dry EtOH and was added drop wise to the previously prepared surfactant solution and the whole mixture was kept under constant stirring at room temperature. After an hour mild aqueous sodium hydroxide solution was added into the mixture to maintain the pH at ca. 11.0. The resulting basic mixture was kept under vigorous stirring for another 2 h. The whole gelatinous mass was then transferred to an autoclave and allowed for hydrothermal treatment at 150 $^0$C for 72 h under static condition. The off-white colored solid material was recovered after through filtration, washed several times with plenty of water and dried under vacuum at room temperature. The optimum molar ratio of the chemical constituents of the synthesis gel was as follows:

Z : TEOS : CTAB : TA : $H_2O$ = 1 : 1 : 1.4 : 0.5 : 90

The material was allowed to undergo solvent extraction with ethanol-HCl mixture for 2 h at room temperature for the removal of CTAB surfactant. Similar synthetic procedure was repeated in another batch where only Z was used as Si precursor (without TEOS).

The peaks marked by asterisks (*) in solid state $^{13}$C CP MAS NMR spectrum are due to the residual template molecules and they are arising from the methylene groups and C1 carbon atoms of the hexadecyl group of the CTAB molecules.

**$Hg^{+2}$ adsorption studies:**

Optimization of adsorbent dosage was done by four adsorption experiments using DMTZ-PMO as adsorbent. To a 25 ml of 2 ppm mercury solution, 10 mg of adsorbent was added onto it and stirred at 1000 rpm for 1 h. Then the solution was centrifuged to filter up the adsorbent and the final solution was analyzed through ICP-OES. Same procedure was repeated for another three times by using 15 mg, 20 mg and 25 mg of DMTZ-PMO adsorbent. For 10 and 15 mg of adsorbent the concentration of the final solution becomes 18 ppb and 7 ppb respectively. But, that for 20 and 25 mg of adsorbent the concentration of Hg(II) was reached below the 2 ppb level. Applying even higher adsorbent dosage, no further improvement in the reduction of the concentration of $Hg^{+2}$ was observed. In the next stage, a typical experiment is performed by dispersing 20 mg of DMTZ PMO in 25 ml of 2 ppm $Hg^{+2}$ aqueous solutions and the whole solution was stirred at 1000 rpm at room temperature. After specific time intervals, 2 ml aliquots of the mixture was taken very quickly

from the system and immediately filtered through centrifugation. The treated aqueous $Hg^{+2}$ solutions were then analyzed using ICP-OES. For methyl mercury adsorption study, 500, 200 and 75 ppb $CH_3HgI$ solution was prepared. 25 ml of each solution was taken with 20 mg adsorbent and aliquots were collected at different time interval. It was observed that the removal efficiency was less in the case of $CH3Hg^{+}$. So the catalyst dosage was increased. The optimized result was obtained with 35 mg adsorbent taken in 25 mL 200 ppb solution. $Hg^{+2}$ removal capacity at different time interval was calculated by using the following equation:

$$R(\%) = \frac{C_0 - C_t}{C_0} \times 100$$

Where R (%) denotes the $Hg^{+2}$ removal efficiency, $C_0$ (mg/L) is the initial $Hg^{+2}$ concentration when adsorbent is just added, and $C_t$ (mg/L) is the $Hg^{+2}$ concentration of the solution at time t (min).

**Estimation of $q_t$ and $q_e$:**

The amount of the $Hg^{+2}$ adsorbed by the material at time t was measured by the equation:

$$q_t = \frac{v}{m} (C_0 - C_t) \quad (1)$$

Where $C_0$ and $C_t$ denotes initial concentration of the $Hg^{+2}$ and that of after time t (min) respectively. V denotes the volume of the aqueous $Hg^{+2}$ solution used for the experiment and m is the mass of the adsorbent material used. By using the intercept from the equation (1), we could obtain the $q_e$ values.

**Mercury vapor adsorption study:**

In an autoclave two glass vials are placed. In one vial 20 mg DMTZ-PMO was taken and in another vial two drop of liquid metallic mercury was taken. The autoclave was closed and placed in a 150 $^0$C oven to get a mercury vapour saturated environment for 4 h. After 4 h, the autoclave was cooled to room temperature, the weight gained by the adsorbent was measured. To find the exact Hg content the adsorbent was dissolved in aqua regia and measured in ICP-OES.

**Regeneration of adsorbent and recyclability**:

The adsorbent was recycled after collection of the sample DMTZ-PMO through filtration and then washed with plenty of water. Then it was washed with plenty of 2N HCl. DMTZ-PMO was then dried under vacuum at 100 °C. Then the adsorbent was reused for the next run for Hg(II) removal.

**Effect of metal cations:**

A stock solution was prepared with nitrate salt of Na, k, Cu, Zn, Co, Ni, Pb, Hg, Cd with concentration 2 ppm of each metal ion. To a 200 ml solution of the same 75 mg DMTZ-PMO was added and stirred for 4 h at room temperature. The concentration of the metal ions were checked using ICP-OES after filtration and separation of the adsorbent.

## Section S2

**Characterization techniques and instrumentation:**

$^{1}$H NMR spectrum of the organosilane monomer was recorded on Bruker ASC End TM 400 MHz NMR spectrometer. FT-IR spectroscopic analysis was carried out in Perkin Elmer Spectrum 100 FTIR spectrometer. Powder X-ray diffraction pattern were measured with a Bruker D8 Advance X-ray diffractometer using Ni-filtered Cu Kα ($\lambda$ = 0.15406 nm). Nitrogen adsorption/desorption experiment was performed with an Autosorb–iQ surface area analyzer at 77 K. The sample was degassed in vacuum at 150 $^{0}$C for 5 h prior to BET measurement to remove all the adsorbed guest molecules inside the pores. The specific surface area was estimated by using Brunaur-Emmett-Teller (BET) model and the pore size distribution was measured by nonlocal density functional theory (NLDFT) method from adsorption/desorption isotherm. Elemental analysis (C, H, N and S) were carried out on a Perkin Elmer 2400 series-II CHN analyzer. 11.74 T Bruker Advanced-II 500 MHz NMR spectrometer equipped with a 4 mm MAS probe of spinning rate 11 KHz was employed for solid state 29Si and 13C CP-MAS NMR spectroscopic analyses. JEOL JEM-2100F transmission electron microscope with operating voltage 200 KV equipped with a FEG provided ultra-high resolution transmission electron microscopic (FEG-TEM) images. Morphology of the particles was determined by taking field-emission scanning electron microscopic images by using a JEOL JSM-7500F. X-ray photoluminescence spectroscopic (XPS) data was recorded in an

Omicron Nanotechnology GmbH XPS machine. The sample was prepared by drop-casting the sample suspension in methanol on a glass slide followed by degassing it for overnight.

The complex of the ligand with a different number of $Hg^{2+}$ ions has been optimised using Gaussian 16 suites of the program. The ab-initio quantum chemical calculation coupled with atoms in molecules (AIM) analysis have been used previously to illustrate non-covalent interactions. In this study we have used range separated, and dispersion corrected wB97XD density functional (capable of describing both short-range and long-range interactions very reliably) and 6-31+G(d) coupled with basis set for the optimization. Dispersion corrected methods are exceptionally reliable in revealing weak non-covalent interaction present in the system. For C, H, N and S we have used 6-31+G(d) basis function whereas we have applied Lan L2DZ basis function and effective core potential for the heavy $Hg^{2+}$ which found to produce a reliable result in earlier studies. During optimisation, we have employed the frozen core approximation and tight convergence criterion. Harmonic frequency calculations have been performed to ensure that all the structures are at local minima. The stabilisation energy for the complexes have been calculated based on the following equation

$$\Delta E_{Stab} = \Delta E_{Comp} - \Delta E_{Hg2+} - \Delta E_{Lig} \qquad (2.1)$$

Where, $\Delta E_{Comp}$, $\Delta E_{Hg2+}$ and $\Delta E_{Lig}$ are zero-point vibrational (ZPV) corrected energies of the complex, the $Hg^{2+}$, and the ligand.

To evaluate the nature of a different kind of non-covalent interactions AIM analysis has been performed and molecular density map generated using Atoms in Molecules (AIM) software. Further, electron density (ρ) and Laplacian of electron density ($\nabla^2 \rho, L$) have been calculated at each bond critical points (BCPs) to understand the nature of the interaction between two interacting atoms. It is important to note that only those BCPs have been considered whose ρ and L are higher than 0.002 and 0.02 a.u., respectively, as they confirm the existence of non-covalent interaction. To measure the strength of any interaction we have calculated the ellipticity of the interaction ($\varepsilon$) at the bond critical point (BCP) using the following equation

$$\varepsilon = \frac{\lambda_1}{\lambda_2} - 1 \qquad (2.2)$$

Where $\lambda$'s are the negative vectors associated with the hessian of $\rho$ at that CP and $\lambda_2 \leq \lambda_1$.

Based on the possibility of interactions between $Hg^{2+}$ and different non-covalent interacting sites of the ligand different conformations up to 3:1 molar ratio between $Hg^{2+}$ and the ligand site was generated. Using wB97XD/6-31+G(d) LanL2DZ(Hg) density function theory, optimization of all the complexes was done, their zero-point vibrational energy (ZPV) corrected stabilization energy (Figure S6) was calculated. Among the possible ratios most stable conformations are A1 and B1, 2:1 B1 complex as insides only within figure 6 for clarity. The stabilization energy is positive for the complex up to 2:1 molar ratio after which it becomes negative (C1) indicates the ligand can easily accommodate up to two $Hg^{2+}$ ions. To measures the anisotropy of the curvature of the electron density at a BCP, ellipticity (ε) at the BCPs for $Hg^{2+}$….O/N/S/H─C of all the complexes (A1-A5, B1-B6) was calculated (Table S2). Higher values of ε mean higher electron density at the perpendicular direction of the interacting plane at that BCP; higher $\pi$ character of the bond. We calculated the electron density (r), Laplacian of electron density (r2 r) and ellipticity (e) at different bond critical points (BCPs) for all the mercuric complexes (A1–A5 and B1–B6) (Fig. S14) and tabulated all topological parameters (Table S2).

## Figure S1

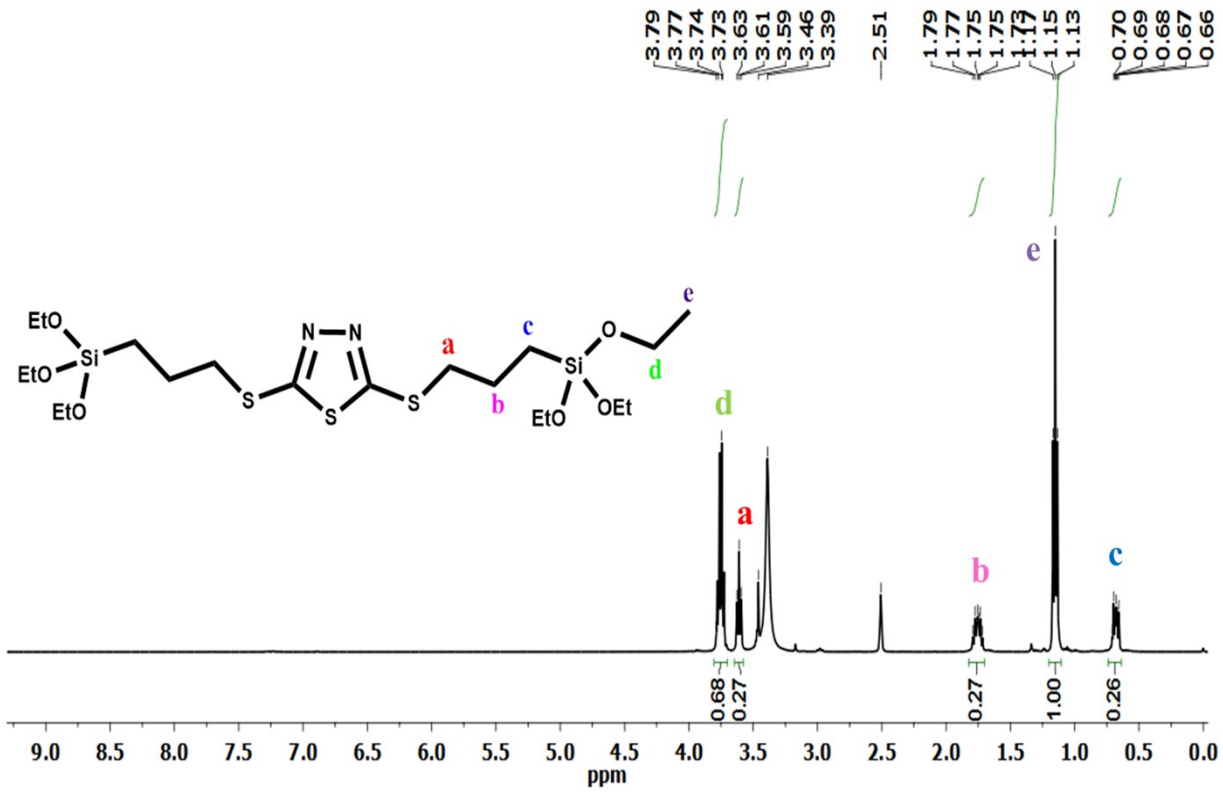


**Figure S1:** $^{1}$H NMR of the organosilane precursor.

**Figure S2**

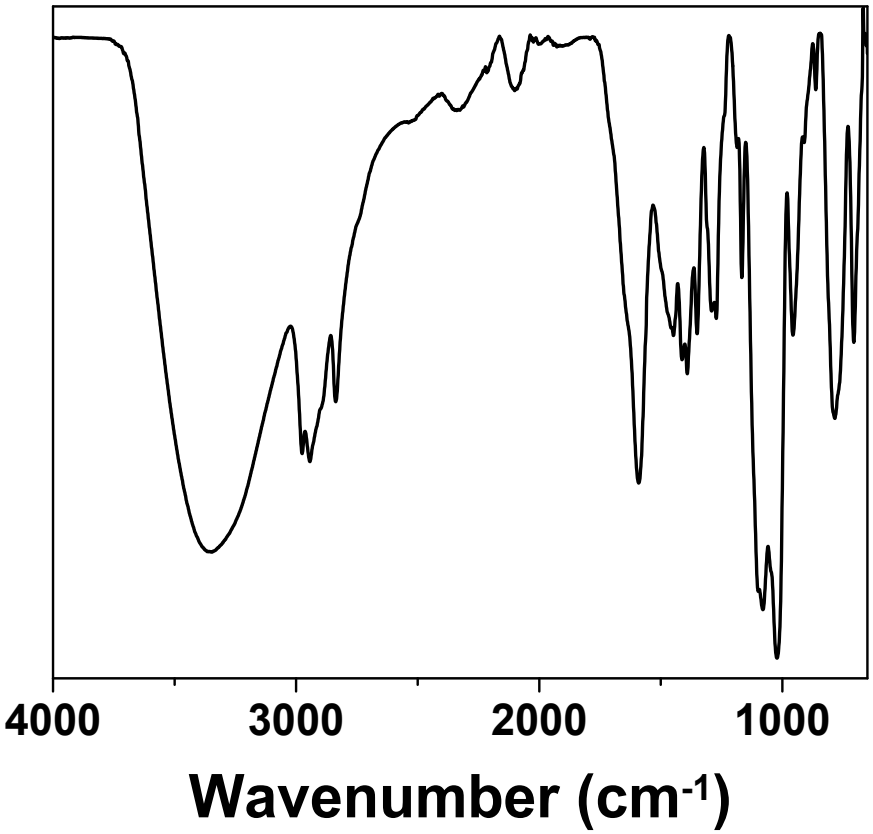


**Figure S2:** FTIR of the organosilane precursor Z.

**Figure S3**

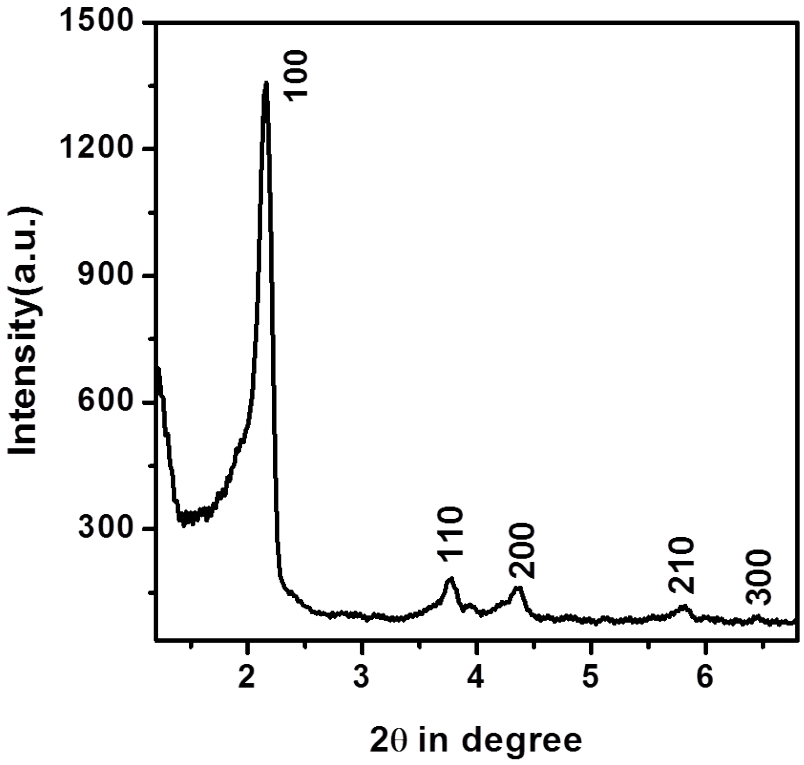


**Figure S3:** Powder XRD of the template free DMTZ-PMO.

## Figure S4

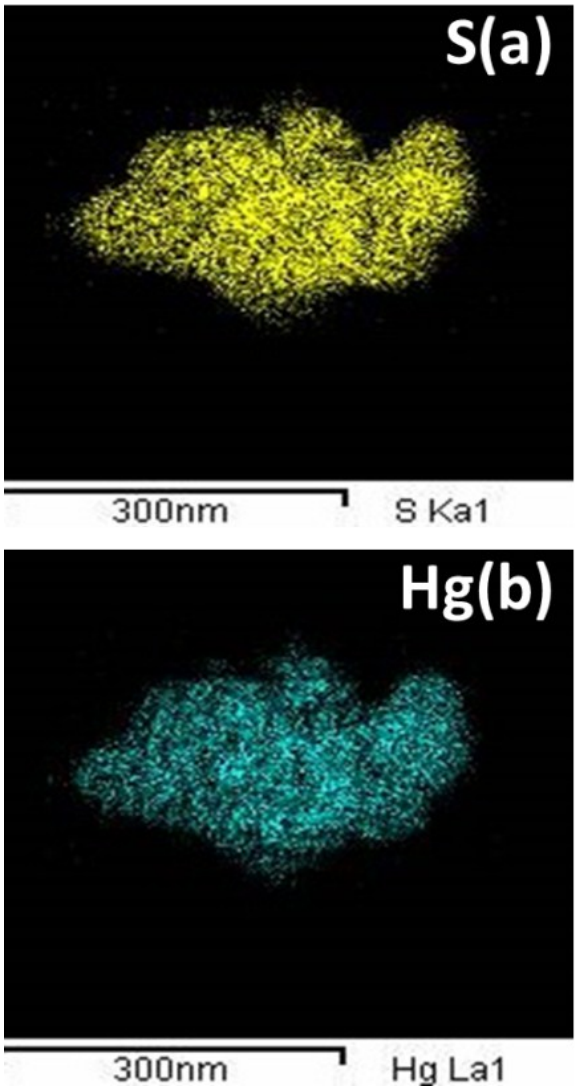


**Figure S4:** Energy-dispersive X-ray analysis (EDS) of the mercury adsorbed DMTZ-PMO.

# Figure S5

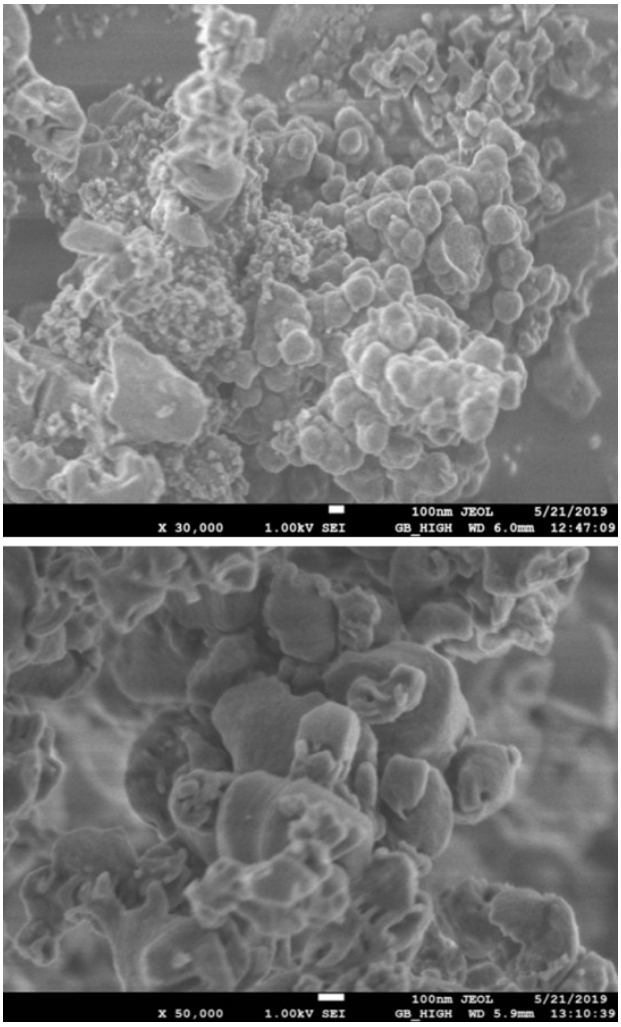


**Figure S5:** FE-SEM images of DMTZ-PMO at different magnifications.

## Figure S6

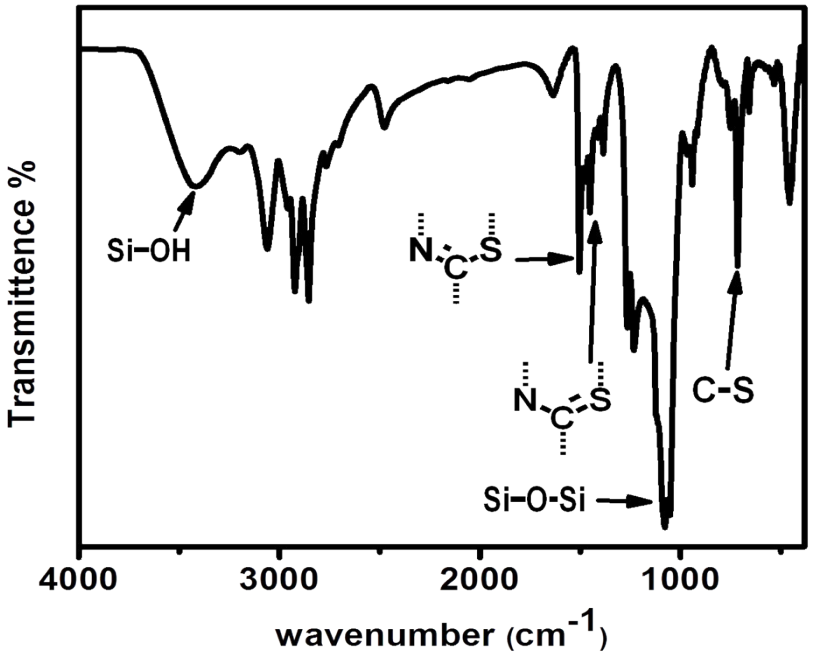


**Figure S6:** FT-IR spectrum of DMTZ PMO.

**Figure S7**

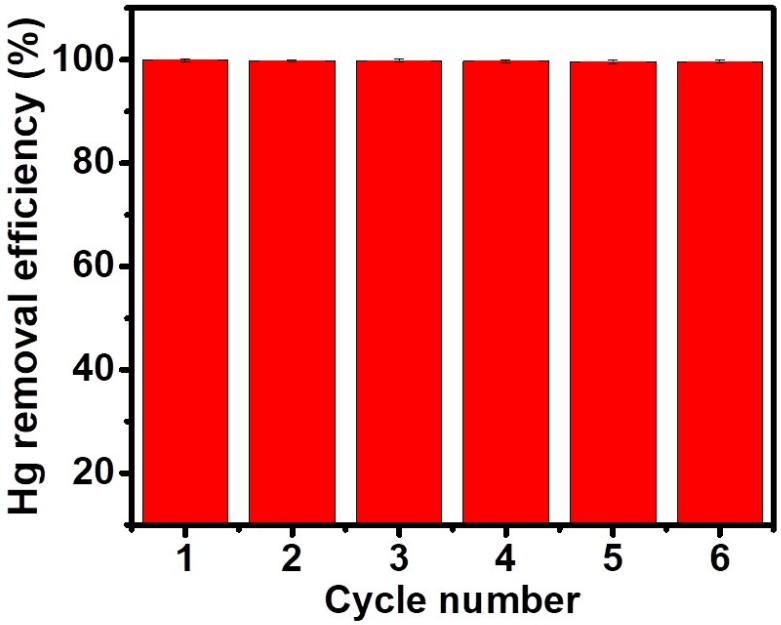


**Figure S7:** Hg(II) removal efficiency for DMTZ-PMO for six consecutive adsorption cycles. Error bars are shown for the uptakes of each cycle.

**Figure S8**

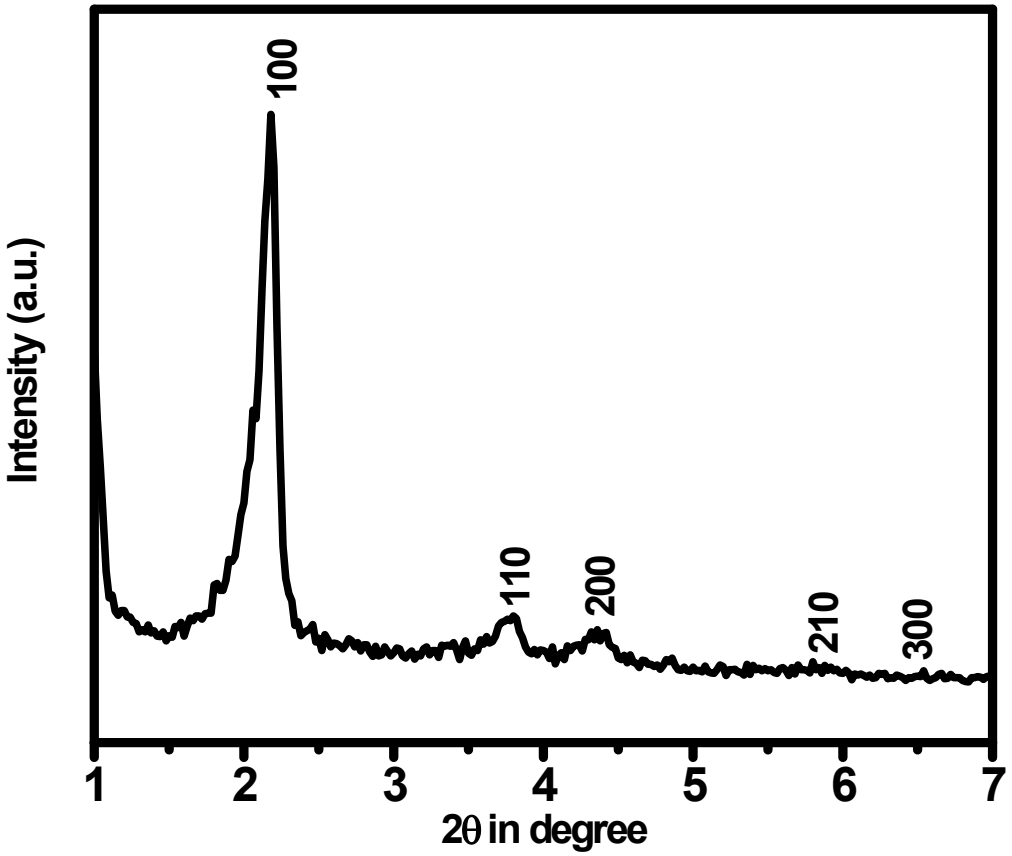


**Figure S8:** Powder XRD of the DMTZ-PMO after six adsorption cycles.

Figure S9

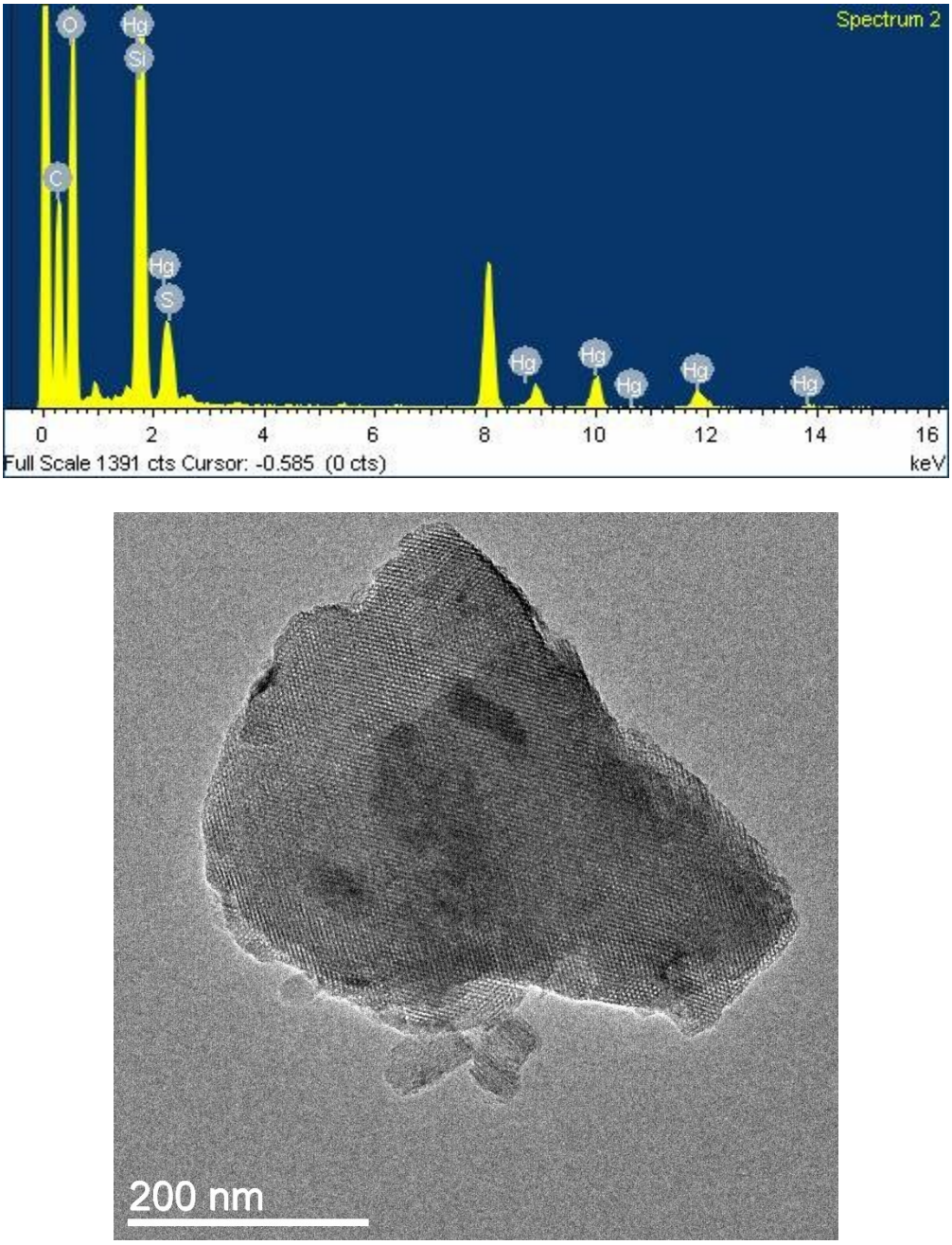


**Figure S9:** EDX analysis and HR TEM image of DMTZ-PMO after Hg(II) adsorption.

## Figure S10

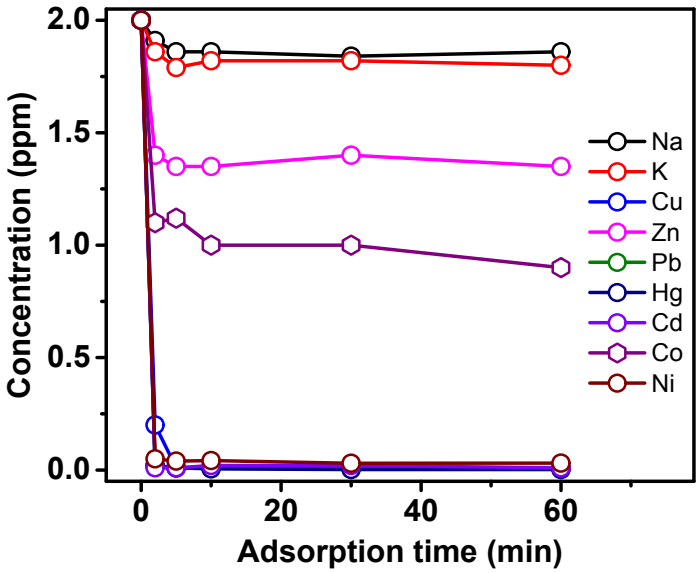


**Figure S10:** Hg(II) removal efficiency in presence of other metal cations.

## Figure S11

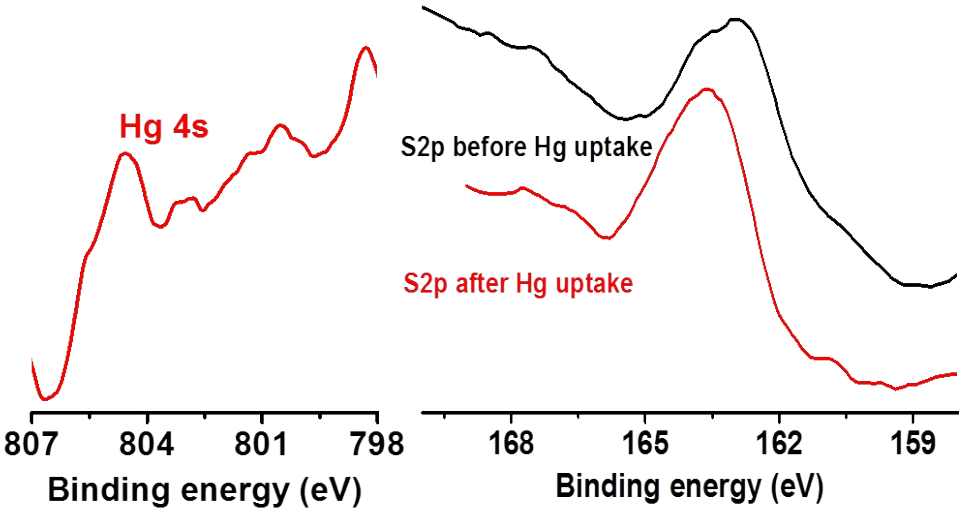


**Figure S11**: XPS plots for short range scan for Hg4s (left) and S2p (before and after Hg adsorption, right) for the material DMTZ-PMO.

# Figure S12

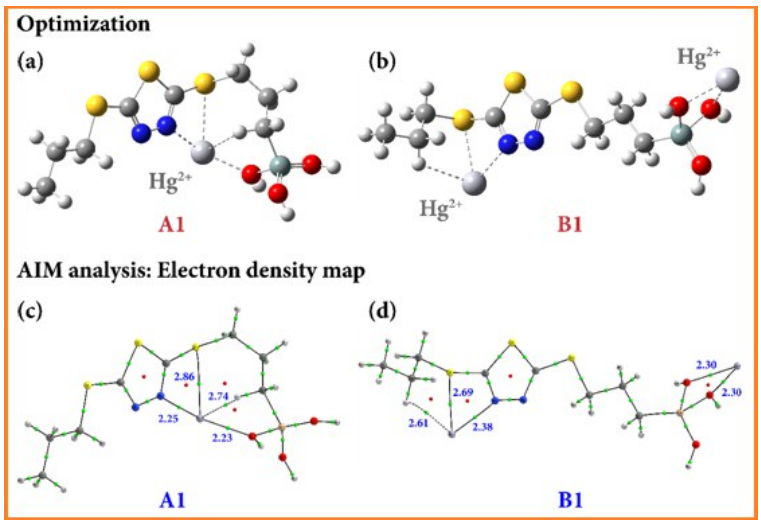


**Figure S12:** (a) Optimized most stable conformers of 1:1 (A1) complex, (b) 2:1 (B) complex. (c) The electron density map of A1 and (d) for B1. A green sphere indicates bond critical point (BCP) and red spheres indicate ring critical point (RCP). The spheres in white =H, yellow=S, red=O, grey=C, light pink=Si, blue=N, and light grey=Hg. Distance between interacting atoms are all in Å unit.

## Figure S13

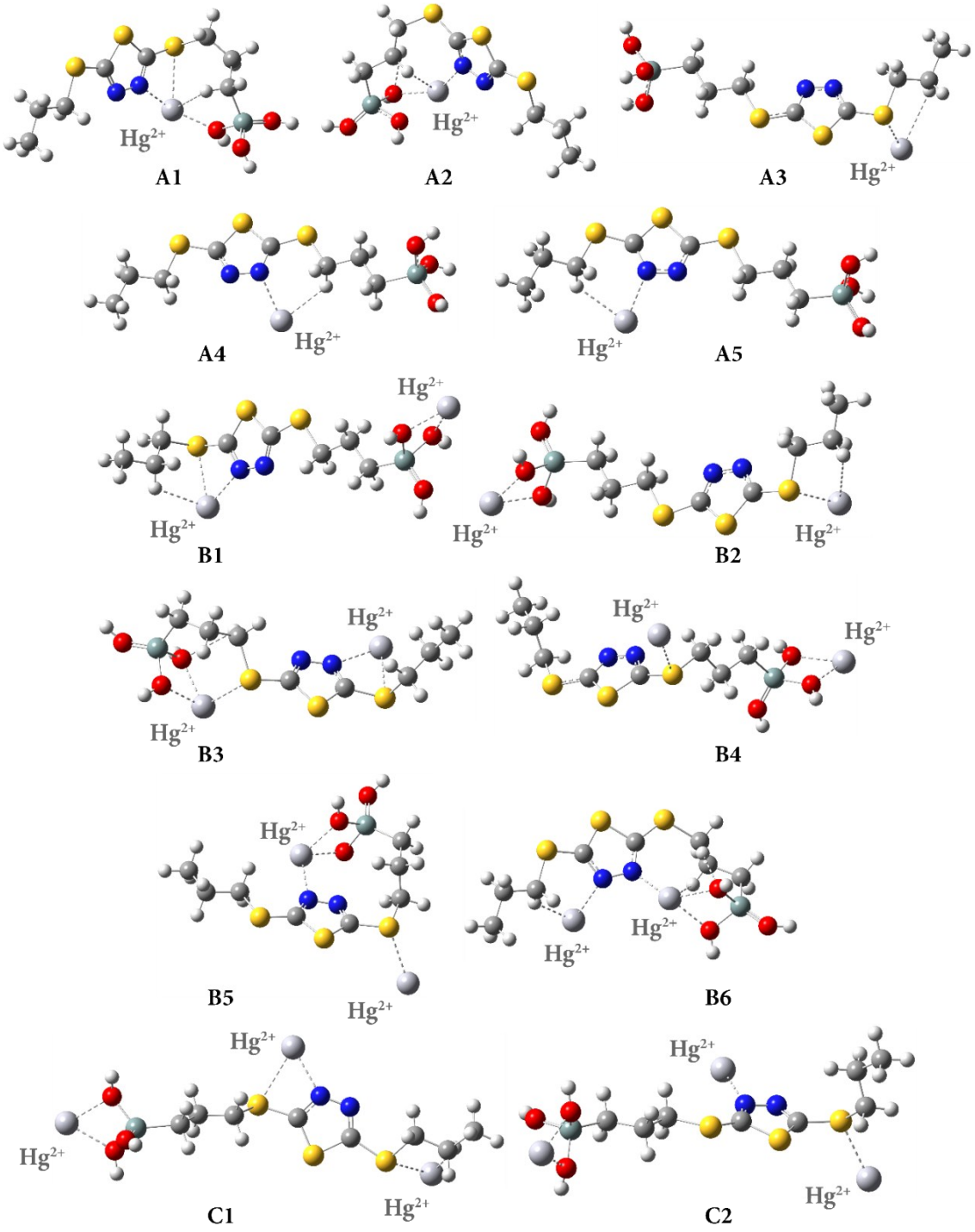


**Figure S13:** Optimized geometry of the complex between $Hg^{2+}$ and the ligand has been shown in 1:1 molar ratio A1-A3 (row 1), A4-A5 (row 2), 2:1 molar ratio B1-B2 (row 3), B3-B4 (row 4), B5-B6 (row 5), and 3:1 molar ratio C1-C2 (row 6) The spheres in white represents H, yellow=S, grey=C, light blue=Si, blue=N, red=O and light grey=Hg.

## Figure S14

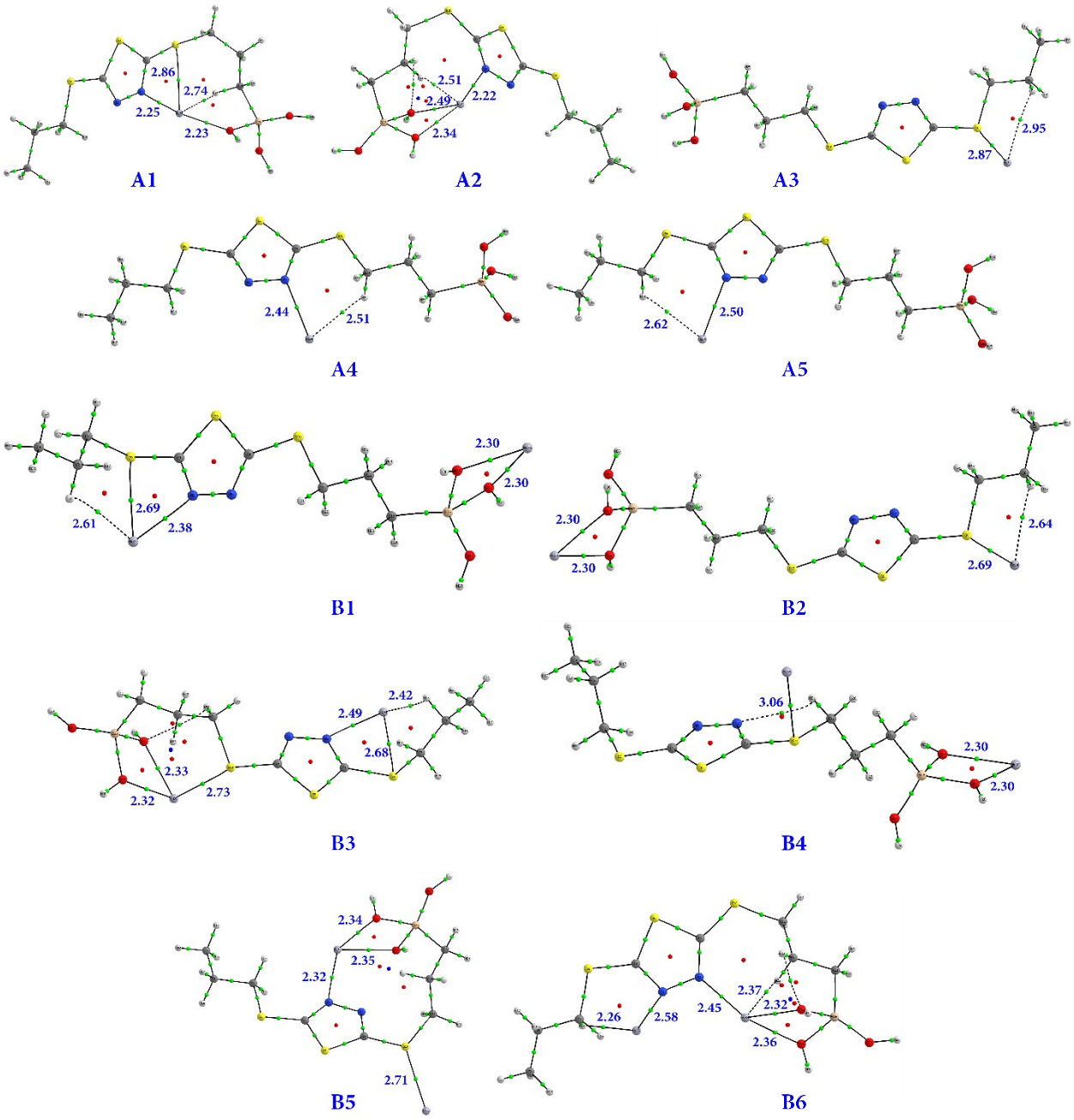


**Figure S14:** Electron density map of all (A1-A5, B1-B6) complexes where green spheres indicate the bond critical point (BCP) that of red is ring critical point (RCP), calculated at wB97XD/6-31+G(d):LanL2DZ(Hg) level of theory. The spheres in white represents H, yellow=S, red=O, grey=C, light pink=Si, blue=N, and light grey=Hg. All distance between interacting atoms is in Å unit. The presence of very strong $Hg^{2+}$…O, $Hg^{2+}$…S, and $Hg^{2+}$…N interaction explains very high stabilisation energy.

# Table S1

| **Type of interactions** | **Distance (Å)** | $\rho$ | $\nabla^2\rho$ | $\varepsilon$ | $\Delta E_{Stab}^{ZPE}$ **(kcal/mole)** |
|---|---|---|---|---|---|
| **A1** | | | | | |
| **$Hg^{2+}$….O** | 2.23 | 0.067 | 0.282 | 0.067 | + 204.7 Stable Complex |
| **$Hg^{2+}$….N** | 2.25 | 0.075 | 0.236 | 0.079 | |
| **$Hg^{2+}$….S** | 2.86 | 0.035 | 0.086 | 0.034 | |
| **$Hg^{2+}$…H─C** | 2.74 | 0.011 | 0.039 | 0.488 | |
| **B1** | | | | | |
| **$Hg^{2+}$….O** | 2.30 | 0.058 | 0.237 | 0.071 | + 166.8 Stable Complex |
| **$Hg^{2+}$….O** | 2.30 | 0.058 | 0.238 | 0.071 | |
| **$Hg^{2+}$….N** | 2.38 | 0.056 | 0.188 | 0.070 | |
| **$Hg^{2+}$….S** | 2.69 | 0.049 | 0.098 | 0.031 | |
| **$Hg^{2+}$…H─C** | 2.61 | 0.015 | 0.045 | 0.277 | |
| **C1** | | | | | - 62.2 Unstable Complex |

**Table S1**: List of stabilization energy ($\Delta E_{stab}$ kcal/mole), electron density ($\rho$, a.u.), Laplacian of electron density ($\nabla^2 \rho$, a.u.), and ellipticity (ε) at the BCPs for different non-covalent interaction for A1 and B1.

# Table S2

| Type of interaction | Distance (Å) | $\rho$ | $\nabla^2\rho$ | $\varepsilon$ | $\Delta E_{Stab}^{ZPE}$ (kcal /mole) |
|---|---|---|---|---|---|
| **A1** | | | | | |
| **$Hg^{2+}$…O** | 2.23 | 0.067 | 0.282 | 0.067 | 204.7 |
| **$Hg^{2+}$…N** | 2.25 | 0.075 | 0.236 | 0.079 | |
| **$Hg^{2+}$…S** | 2.86 | 0.035 | 0.086 | 0.034 | |
| **$Hg^{2+}$…H─C** | 2.74 | 0.011 | 0.039 | 0.488 | |
| **A2** | | | | | |
| **$Hg^{2+}$…O** | 2.49 | 0.037 | 0.153 | 0.064 | 197.7 |
| **$Hg^{2+}$…O** | 2.34 | 0.052 | 0.214 | 0.064 | |
| **$Hg^{2+}$…N** | 2.22 | 0.080 | 0.249 | 0.069 | |
| **$Hg^{2+}$…H─C** | 2.51 | 0.019 | 0.074 | 3.466 | |
| **A3** | | | | | |
| **$Hg^{2+}$…O** | 2.87 | 0.035 | 0.067 | 0.064 | -157.9 |
| **$Hg^{2+}$…H─C** | 2.95 | 0.008 | 0.022 | 0.554 | |
| **A4** | | | | | |
| **$Hg^{2+}$…N** | 2.44 | 0.050 | 0.152 | 0.091 | 156.1 |
| **$Hg^{2+}$…H─C** | 2.51 | 0.018 | 0.051 | 0.168 | |
| **A5** | | | | | |
| **$Hg^{2+}$…N** | 2.50 | 0.044 | 0.133 | 0.094 | 154.4 |
| **$Hg^{2+}$…H─C** | 2.62 | 0.014 | 0.040 | 0.177 | |
| **B1** | | | | | |
| **$Hg^{2+}$…O** | 2.30 | 0.058 | 0.237 | 0.071 | 166.8 |
| **$Hg^{2+}$…O** | 2.30 | 0.058 | 0.238 | 0.071 | |
| **$Hg^{2+}$…N** | 2.38 | 0.056 | 0.188 | 0.070 | |
| **$Hg^{2+}$…S** | 2.69 | 0.049 | 0.098 | 0.031 | |
| **$Hg^{2+}$…H─C** | 2.61 | 0.015 | 0.045 | 0.277 | |
| **B2** | | | | | |
| **$Hg^{2+}$…O** | 2.30 | 0.058 | 0.238 | 0.071 | 155.5 |
| **$Hg^{2+}$…O** | 2.30 | 0.058 | 0.238 | 0.071 | |
| **$Hg^{2+}$…S** | 2.69 | 0.049 | 0.085 | 0.065 | |
| **$Hg^{2+}$…H─C** | 2.64 | 0.014 | 0.042 | 0.331 | |
| **B3** | | | | | |
| **$Hg^{2+}$…O** | 2.33 | 0.054 | 0.223 | 0.066 | 149.0 |
| **$Hg^{2+}$…O** | 2.32 | 0.054 | 0.228 | 0.077 | |
| **$Hg^{2+}$…S** | 2.73 | 0.045 | 0.099 | 0.050 | |
| **$Hg^{2+}$…N** | 2.49 | 0.043 | 0.148 | 0.057 | |
| **$Hg^{2+}$…S** | 2.68 | 0.050 | 0.100 | 0.045 | |
| **$Hg^{2+}$…H─C** | 2.42 | 0.021 | 0.061 | 0.167 | |
| **B4** | | | | | |
| **$Hg^{2+}$…O** | 2.30 | 0.057 | 0.238 | 0.080 | 132.5 |
| **$Hg^{2+}$…O** | 2.30 | 0.057 | 0.235 | 0.081 | |
| **$Hg^{2+}$…S** | 3.06 | 0.026 | 0.050 | 0.060 | |
| **B5** | | | | | |
| **$Hg^{2+}$…O** | 2.34 | 0.052 | 0.217 | 0.077 | 120.2 |

| | | | | | |
|---|---|---|---|---|---|
| **$Hg^{2+}$…O** | 2.35 | 0.051 | 0.211 | 0.069 | |
| **$Hg^{2+}$…N** | 2.33 | 0.062 | 0.213 | 0.080 | |
| **$Hg^{2+}$…S** | 2.71 | 0.048 | 0.082 | 0.061 | |
| **B6** | | | | | |
| **$Hg^{2+}$…O** | 2.32 | 0.055 | 0.224 | 0.063 | 91.0 |
| **$Hg^{2+}$…O** | 2.36 | 0.051 | 0.207 | 0.058 | |
| **$Hg^{2+}$…H─C** | 2.37 | 0.024 | 0.091 | 0.818 | |
| **$Hg^{2+}$…N** | 2.45 | 0.049 | 0.160 | 0.097 | |
| **$Hg^{2+}$…N** | 2.58 | 0.038 | 0.105 | 0.106 | |
| **$Hg^{2+}$…H─C** | 2.26 | 0.030 | 0.073 | 0.103 | |
| **C1** | | | | | -62.2 |
| **C2** | | | | | -88.0 |

**Table S2:** List of stabilization energy ( $\Delta E_{Stab}$ , kcal/mole), electron density ( $\rho$ a. u.), Laplacian of electron density ( $\nabla^2\rho$ a. u.), and Ellipticity (ε) at the BCPs of the different non-covalent interaction of the mercuric complexes (A1-A5, B1-B6) calculated at wB97XD/6-31+G (d):LanL2DZ (Hg) level of theory.